Journal of Pharmaceutical Analysis 14 (2024) 100967

Contents lists available at ScienceDirect

Journal of Pharmaceutical Analysis

journal homepage: www.elsevier.com/locate/jpa

Short communication

Establishment of microneurovascular units in alginate hydrogel microspheres to reveal the anti-hypoxic effect of salidroside

Shiyu Chen [a, b], Yuxuan Li [b], Yingrui Zhang [a, b], Hongren Yao [b], Tong Xu [a, b], Yi Zhang [c], Jin-Ming Lin [b, **], Xian-Li Meng [a, *]

[a] State Key Laboratory of Southwestern Chinese Medicine Resources, Innovative Institute of Chinese Medicine and Pharmacy, Chengdu University of Traditional Chinese Medicine, Chengdu, 611137, China
[b] Beijing Key Laboratory of Microanalytical Methods and Instrumentation, Department of Chemistry, Key Laboratory of Bioorganic Phosphorus Chemistry & Chemical Biology (Ministry of Education), Tsinghua University, Beijing, 100084, China
[c] School of Ethnic Medicine, Chengdu University of Traditional Chinese Medicine, Chengdu, 611137, China

ARTICLE INFO

Article history:
Received 21 January 2024
Received in revised form
14 March 2024
Accepted 18 March 2024
Available online 20 March 2024

Microneurovascular units (mNVUs), comprising neurons, microglia, and blood-brain barrier (BBB) endothelial cells, are pivotal to the central nervous system and are associated with cerebral hypoxia and brain injuries. Cerebral hypoxia triggers microglial overactivity, causing inflammation, neuronal injury, and disruption of the BBB [1]. Salidroside (Sal), a key compound in Tibetan medicine *Rhodiola crenulata*, mitigates hypoxia-induced metabolic disorders and neuronal damage by preserving mitochondrial function [2]. A method combining a three-dimensional (3D) simulated microenvironment with precise detection is needed to accurately understand the anti-hypoxic effects of drugs such as Sal using *in vitro* models, due to the simplicity of traditional monolayer cell cultures and the complexity of animal experiments [3]. We propose using an alginate hydrogel microsphere (AHMs)-based microfluidic approach for constructing mNVUs with BV2 microglia and HT22 neurons. The 3D microenvironment minimized shear stress, aiding precise control. Our method exposed mNVUs to a hypoxic microenvironment using deferoxamine (DFO), simulating overactivated microglia and injured neurons. Quantitative analysis of changes in metabolite content in the tricarboxylic acid (TCA) cycle was performed using mass spectrometry (MS) and metabolism of the Sal to evaluate the anti-hypoxic efficacy of Sal and the mechanism underlying anti-hypoxic inflammation through the nuclear factor-kappa B (NF-κB) pathway. This biofriendly, compatible platform is a potent tool for assessing cellular metabolism and brain protection drug screening, uncovering evident mNVU interactions through comparative HT22 and BV2/HT22 co-culture.

The HT22-BV2 core-shell structure in AHMs was an mNVU, which provided detailed metabolic insights. The "Experimental section" is shown in the Supplementary data. Sal reversed DFO-induced glycolytic shift to oxidative phosphorylation (Fig. S1). The microfluidic chip (Figs. S2A and B) comprises a custom device that connects a syringe to an infusion pump. BV2 and HT22 cells-laden alginate hydrogels were injected through inlets, resulting in the formation of outer (BV2) and inner (HT22) layers. Laminar flow was visualized (Figs. S2C and D). The dispersed phase utilized ethylenediaminetetraacetic acid-calcium (EDTA-Ca) complex with alginate. The continuous phase was fluorocarbon oil with surfactant. Convergence at the first cross-channel led to the formation of gelation and AHM. H^+ diffusion resulted in the solidification of AHMs into pre-microgel spheroids. Bulk AHMs escaped the oil-water interface for incubation. Optimal fluid conditions yielded AHMs with a diameter of 250 μm (Figs. S3A–C). A 2% concentration of sodium alginate maintained long-term culture without easy breakage. The cells exhibited excellent activity and a clear core-shell structure of the hydrogel microspheres (Figs. S3D and E). Ultra-performance liquid chromatography-tandem mass spectrometry (UPLC-MS/MS) was performed to determine Sal's efficacy on mNVUs and analyze differences in TCA cycle metabolism between HT22 monoculture and HT22-BV2 co-culture. Appropriate amounts of cells were loaded into high-throughput core-shell AHMs to evaluate Sal's efficacy. The collected AHMs were transferred for culture, and cells in the AHMs maintained high viability for at least three days (Figs. 1A and B). HT22 and BV2 cells aggregated within AHMs. Proper DFO concentration was crucial for establishing a hypoxic inflammation model. The Cell Counting Kit-8 (CCK-8) assay was used to determine cell viability with Sal or DFO,

* Corresponding author.
** Corresponding author.
E-mail addresses: xlm999@cdutcm.edu.cn (X.-L. Meng), jmlin@mail.tsinghua.edu.cn (J.-M. Lin).

https://doi.org/10.1016/j.jpha.2024.100967

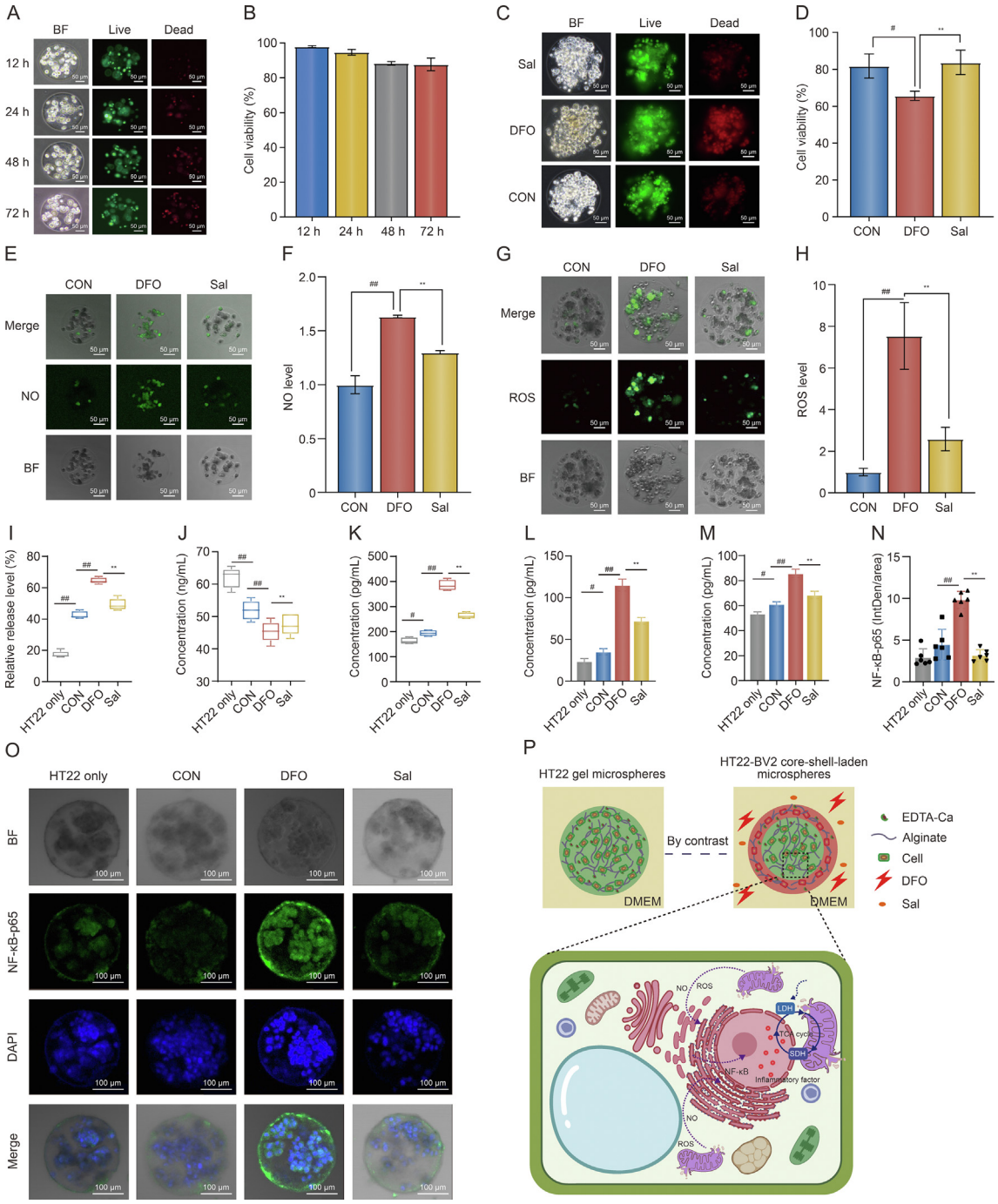

Fig. 1. Fate of microneurovascular units (mNVUs)-laden alginate hydrogel microspheres (AHMs) and changes in corresponding hypoxic metabolic indicators in the tricarboxylic acid (TCA) cycle and downstream inflammatory cytokines of nuclear factor-kappa B (NF-κB) pathway under different culture conditions. (A, B) Fluorescent images (A) and fluorescence intensity (B) of mNVUs-laden AHMs for three days. (C, D) Fluorescent images (C) and fluorescence intensity (D) after co-treatment of salidroside (Sal) (50 μM) and deferoxamine (DFO) (80 μM) for 24 h in the mNVUs-laden AHMs. (E, F) Fluorescent images (E) and fluorescence intensity (F) of cellular nitric oxide (NO) levels in mNVUs-laden AHMs. (G, H) Fluorescent images (G) and fluorescence intensity (H) of cellular reactive oxygen species (ROS) generation in mNVUs-laden AHMs. (I–K) The levels of lactate dehydrogenase (LDH) (I), succinate dehydrogenase (SDH) (J), and hypoxia-inducible factor 1 alpha (HIF-1α) (K) in mono-cultured HT22 cells and mNVUs-laden AHMs under different culture stimulation conditions after 24 h. (L, M) The levels of tumor necrosis factor alpha (TNF-α) (L) and interleukin-6 (IL-6) (M) secreted downstream of the NF-κB pathway in mono-cultured HT22 cells and mNVUs-laden AHMs under different culture stimulation conditions after 24 h. (N, O) Fluorescence intensity (N) and fluorescence image (O) of NF-κB p65 expression under different culture conditions. (P) Differences between mNVUs-laden AHMs and mono-cultured HT22 cells and the mechanistic diagram illustrate the relationship between Sal on DFO-induced hypoxic inflammation and energy metabolism. Data above were presented as mean ± standard deviation (SD) ($n = 3$). $^{\#}P < 0.05$ and $^{\#\#}P < 0.01$, compared to the control group (CON); $^{**}P < 0.01$, compared to the model group. BF: bright field; DAPI: 4′,6-diamidino-2-phenylindole; EDTA: ethylenediaminetetraacetic acid; DMEM: Dulbecco's modified Eagle medium.

confirming Sal's safety at various concentrations (Figs. S4A and B). DFO induction successfully yielded the AHM hypoxia model, and 50 μM Sal counteracted decreased cell viability caused by DFO ($^{\#}P < 0.05$ and $^{**}P < 0.01$) (Figs. 1C, 1D, and S4C–E).

An imbalanced in energy supply causing hypoxia may lead to cellular apoptosis and organ dysfunction. Nitric oxide (NO), a key mediator of hypoxia, regulates various physiological processes, including inflammation. Excessive NO levels during severe hypoxia

induce apoptotic cell death [4]. In a hypoxic environment, electron leakage during oxidative phosphorylation (OXPHOS) generates reactive oxygen species (ROS), causing mitochondrial dysfunction, adenosine triphosphate (ATP) reduction, and increased apoptosis and inflammation. DFO significantly increased NO and ROS levels, effectively reduced by Sal ($^{\#\#}P < 0.01$ and $^{**}P < 0.01$) (Figs. 1E–H). Sal alleviated DFO-induced hypoxic inflammation and affected energy metabolism in mNVUs-laden AHMs. Hypoxia-inducible

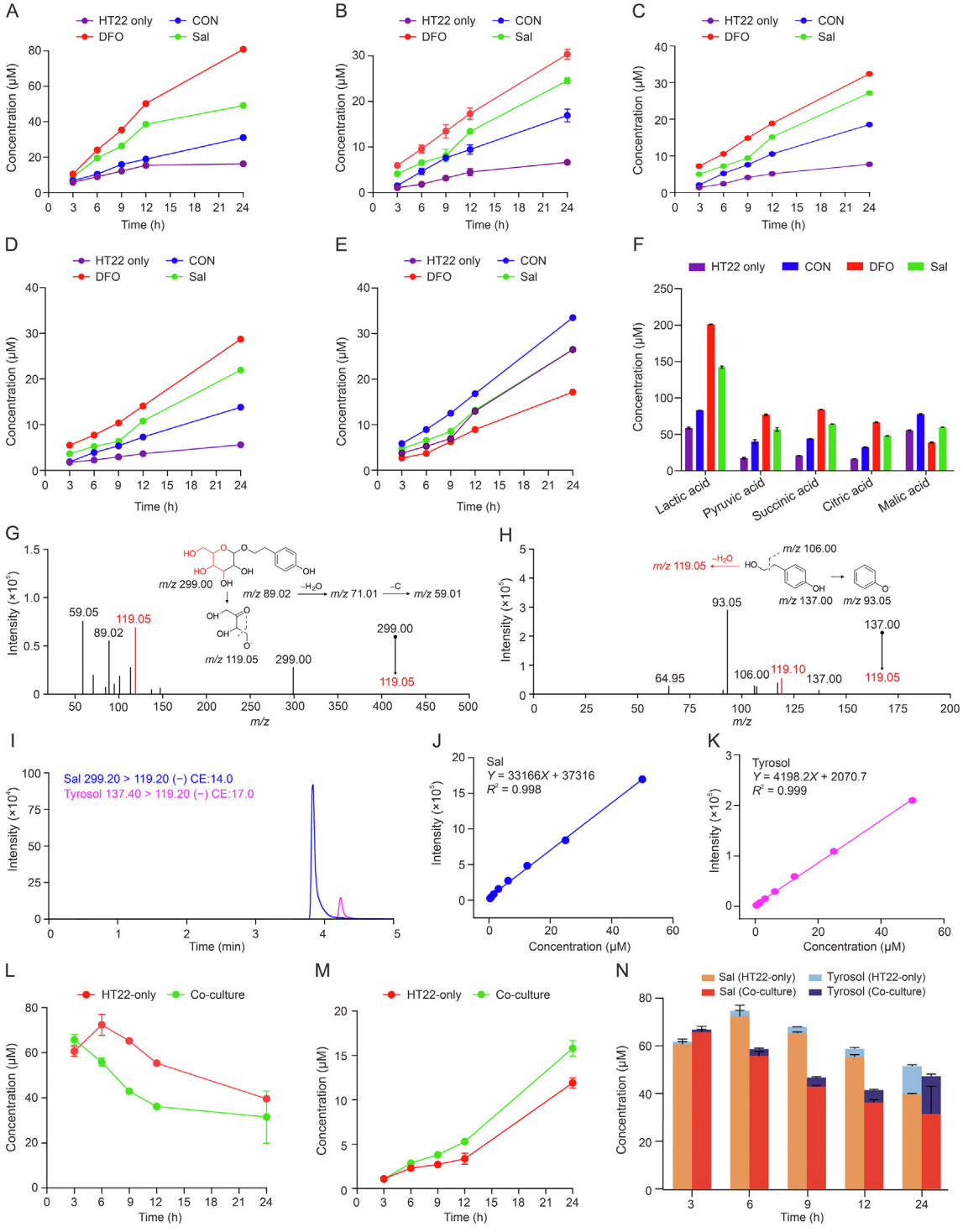

Fig. 2. Time-dependent variations in the levels of the five major metabolites of the tricarboxylic acid (TCA) cycle under different circumstances and characterization of salidroside (Sal) and its metabolite, tyrosol. (A–E) The levels of lactic acid (A), pyruvic acid (B), succinic acid (C), citric acid (D), and malic acid (E). (F) Content variation data for lactic acid, pyruvic acid, succinic acid, malic acid, and citric acid across the four different groups within 24 h. (G) Sal's product ion scan spectra are at *m/z* 299.00 and the peak of the fragment ion is at *m/z* 119.05. (H) The product ion scan spectra of tyrosol are at *m/z* 137.0 and the peak of the fragment ion is at *m/z* 119.05. (I) Representative chromatograms of Sal and its metabolite, tyrosol. (J, K) The calibration curves for Sal (J) and tyrosol (K). (L) Time-dependent variations in Sal-treated microneurovascular units (mNVUs)-laden alginate hydrogel microspheres (AHMs) and mono-cultured HT22 cells. (M) Time-dependent variations in tyrosol-treated mNVUs-laden AHMs and mono-cultured HT22 cells. (N) Sal and tyrosol levels at 24 h in mNVUs-laden AHMs and mono-cultured HT22 cells. Data were presented as mean ± standard deviation (SD) ($n = 3$). CON: control group; DFO: deferoxamine; CE: collision energy.

factor 1 alpha (HIF-1α), a glycolytic regulator, helps cells adapt to hypoxia, promoting a shift toward glycolysis. Lactate dehydrogenase (LDH), involved in anaerobic glycolysis, regulates acid-base balance. Elevated lactate production leads to ROS generation. Succinate dehydrogenase (SDH), a part of the TCA cycle, catalyzes succinic acid oxidation. Sal treatment maintained high SDH levels and reduced DFO-induced decrease in SDH [5]. Sal reduced DFO-induced increases in the levels of LDH, HIF-1α, tumor necrosis factor alpha (TNF-α), and interleukin-6 (IL-6) levels ($^{\#}P < 0.05$, $^{\#\#}P < 0.01$, and $^{**}P < 0.01$) (Figs. 1I–M). Hypoxia led to elevated HIF-1α and LDH levels, further promoting glycolysis, inflammatory cytokines, and lactate expression. Sal suppressed activation of the NF-κB pathway under hypoxia (Figs. 1N and O), and this expression could be suppressed in the Sal group. DFO-induced hypoxia initiated an inflammatory response through the NF-κB pathway in mNVU-laden AHMs, and Sal attenuated the hypoxic damage caused by DFO by inhibiting NF-κB. mNVUs-laden AHMs preferred OXPHOS for metabolism and lower inflammatory responses compared to mono-cultured HT22 cells, indicating that the microenvironment created by AHMs laden with mNVUs is more conducive to cell survival (Fig. 1P). We focused on the differences between the metabolism of HT22 hippocampal neurons induced by hypoxia and metabolic changes in the co-culture system after 24 h. The 24 h incubation medium of mNVUs-laden AHMs was subjected to UPLC-MS/MS analysis, with the medium of monocultured HT22 cells as a control. Compounds of the TCA cycle (lactic acid, pyruvic acid, succinic acid, malic acid, and citric acid) were quantitatively measured, by obtaining peak profiles, scan spectra, and curves (Fig. S5 and Table S1). Four groups of AHMs were fabricated as follows: mono HT22-laden AHMs, BV2-HT22 co-cultured AHMs, DFO-induced BV2-HT22 co-cultured AHMs, and Sal-administered BV2-HT22 co-cultured AHMs. UPLC-MS/MS analysis at 3, 6, 9, 12, and 24 h showed significantly higher levels of lactic acid (Fig. 2A), pyruvic acid (Fig. 2B), succinic acid (Fig. 2C), and citric acid (Fig. 2D) in mNVUs-laden AHMs compared to co-culture and mono HT22-laden AHMs. Their corresponding levels increased in the co-culture group after DFO induction, while Sal treatment downregulated these levels. Malic acid (Fig. 2E) levels decreased 24 h after DFO induction, and Sal increased the malic acid content. mNVUs-laden AHMs exhibited enhanced TCA cycle metabolism. Sal normalized DFO-induced fluctuations (Fig. 2F). We identified the prototype drug and tyrosol, obtaining peak profiles and curves to examine the time-dependent effects of Sal and its metabolites (Figs. 2G–K). Sal uptake was higher in mNVUs-laden AHMs, particularly for tyrosol. The hydrogel co-culture model demonstrated superior drug absorption, better mimicking *in vivo* conditions for accurate clinical pharmacological evaluations (Figs. 2L–N).

In summary, we established an AHM co-culture system using microfluidic technology by assembling BV2 and HT22 hierarchically into a 3D core-shell scaffold. The microtissues, resembling mNVUs, functionally responded to hypoxia. Brain protection by Sal was successfully evaluated via UPLC-MS/MS, revealing its anti-hypoxic inflammation mechanism through the NF-κB pathway. The system analyzed Sal-induced changes in TCA cycle compounds during hypoxic inflammatory diseases. Cells could be easily replaced, enabling diverse model creation. This AHM co-culture system is advantageous for developing *in vitro* neurovascular models and high-throughput screening of anti-hypoxic drugs.

CRediT author statement

Shiyu Chen: Investigation, Conceptualization, Methodology, Data curation, Formal analysis, Writing - Original draft preparation; **Yuxuan Li:** Investigation, Conceptualization, Methodology; **Yingrui Zhang:** Data curation, Formal analysis; **Hongren Yao:** Validation; **Tong Xu:** Visualization; **Yi Zhang**, **Jin-Ming Lin**, and **Xian-Li Meng:** Supervision, Project administration, Funding acquisition, Writing - Reviewing and Editing.

Declaration of competing interest

The authors declare that there are no conflicts of interest.

Acknowledgments

This work was supported by the National Natural Science Foundation of China (Grant Nos.: 82274207, 81973569, and 22034005), the Xinglin Scholar Research Promotion Project of Chengdu University of Traditional Chinese Medicine, China (Grant No.: XKTD2022013), and the Sichuan Provincial Natural Science Foundation, China (Grant No.: 24NSFSC1748).

Appendix A. Supplementary data

Supplementary data to this article can be found online at https://doi.org/10.1016/j.jpha.2024.100967.

References

1 C. Cserép, B. Pósfai, Á. Dénes, Shaping neuronal fate: Functional heterogeneity of direct microglia-neuron interactions, Neuron 109 (2021) 222–240.
[2] F. Fan, N. Xu, Y. Sun, et al., Uncovering the metabolic mechanism of salidroside alleviating microglial hypoxia inflammation based on microfluidic chip-mass spectrometry, J. Proteome Res. 21 (2022) 921–929.
[3] Y. Li, H. Yao, S. Chen, et al., Effect of tryptophan metabolites on cell damage revealed by bacteria-cell interactions in hydrogel microspheres, Anal. Chem. 95 (2023) 1402–1408.
[4] S. Chen, F. Fan, Y. Zhang, et al., Metabolites from scutellarin alleviating deferoxamine-induced hypoxia injury in BV2 cells cultured on microfluidic chip combined with a mass spectrometer, Talanta 259 (2023), 124478.
[5] Y. Zhang, S. Chen, F. Fan, et al., Neurotoxicity mechanism of aconitine in HT22 cells studied by microfluidic chip-mass spectrometry, J. Pharm. Anal. 13 (2023) 88–98.